Deliverable DD-5

Experimental Dataset User Manual

Version 1.1, 24 Nov 2022

Author	Approved	Signature	Date
ESA Acceptance			

Issue	Date	Comments
1.0	22 Sept 2022	First version delivered to CSAO partners
1.1	24 Nov 2022	Update for Sea Level data set v0.3

Change Log

Issue	Author	Affected Section	Change	Status
1.0	JAG (MSSL), SKR (DTU), FG(LEGOS)	All	Document Creation	
1.2	JAG	1, 2.1		

Contents

List of Acronyms

ASA	All Surface Anomaly
ATBD	Algorithm Theoretical Basis Document
CF	Climate and Forecast
CLS	Collecte Localisation Satellites
DAC	Dynamic Atmospheric Correction
DOT	Dynamic Ocean Topography
DTU	Technical University of Denmark
ESA	European Space Agency
GPOD	ESA Grid Processing On Demand
ILA	Ice Level Anomaly
LEGOS	Laboratoire d'Etudes en Géophysique et Océanographie Spatiales
LRM	Low Resolution Mode
MDT	Mean Dynamic Topography
MSS	Mean Sea Surface
MSSL	Mullard Space Science Laboratory
NSIDC	National Snow and Ice Data Center (NSIDC)
OGMOC	Optimal Geoid for Modelling Ocean Circulation
SAMOSA	SAR Altimetry MOde Studies and Applications
SAR	Synthetic Aperture Radar
SARM	SAR Mode
SHA	Surface Height Anomaly
SLA	Sea level Anomaly
SSHA	Sea Surface Height Anomaly
TFMRA	Threshold First Maximum Retracker
UCL	University College London
VR	Validation Report
WP	Work Package

1. Introduction

This document presents the Experimental Dataset User Manual (deliverable DD-5) for the WP5 'Experimental Dataset Generation and Impact Assessment' phase of Cryosat+ Antarctic Ocean (CSAO). The objective of this document is to describe the experimental dataset which is deliverable DD-8.
The aim of CSAO was to explore, develop and validate novel methods to retrieve improved sea-ice freeboard, thickness, ocean surface topography and currents in Antarctica, including in polynyas and leads. It also aimed to define new prototype algorithms for sea-ice freeboard and thickness ground processors and to analyse the resulting datasets in terms of impact on sea ice and ocean dynamics and transport.

The Experimental Dataset is comprised of the Sea Level Product (for the Cryosat mission lifetime 2010 - 2022) and the Sea Ice Product (for 2019) , which cover the Antarctic Ocean. Uncertainty parameters for each ice and ocean measurement are provided.

The format of the products are gridded netCDF, designed to be in compliance with the CF conventions (http://cfconventions.org) and reusing, where possible, existing conventions from CryoSat-2 L2 products.

2. Experimental Dataset Description

2.1. Sea Level Product

2.1.1 Along-track Sea Level Validation

The performance of empirical retrackers going from open ocean (left) to the sea ice cover (right) is illustrated in Figure 1. The lines show different retrackers from the DTU LARS retracking system (see figure caption for more explanation). Retrackers from the DTU LARS retracker system is a system of multiple (empirical) retrackers implemented in C++. The figure shows a variety of the range offsets depending on the retracker. Looking at the median difference between the open ocean and lead observations (Figure 2), it is seen that threshold retracker and the physical retracker SAMOSA+ from GPOD which is processed by the European Space Agency's (ESA) former Grid Processing on Demand (GPOD) SARvatore & SARINvatore service (Dinardo et al., 2016), minimizes the difference between the open ocean and the leads. This GPOD solution is a DTU in-house post processing of the GPOD data.
Figure 3 shows the monthly variation of the standard deviation of the SLA of the retrackers. Here, GPOD clearly outperforms all the retracker, which is due to its stability over the open ocean, where the empirical retrackers suffer.

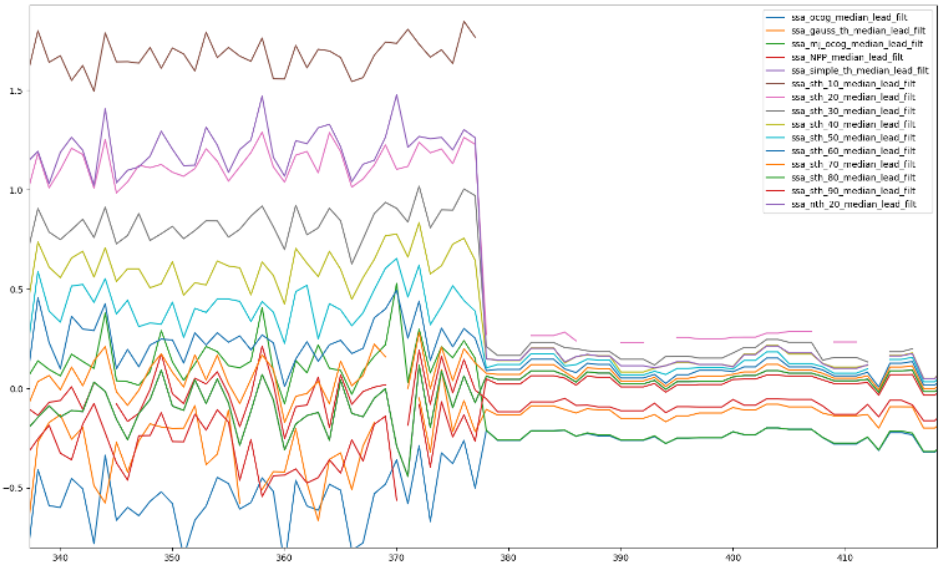

Figure 1. Transition of CryoSat SAR data going from open ocean (left) to the sea ice cover (right) for a variety of retrackers from the DTU LARS retracker system. The Retracker area from top to bottom in the legend: OCOG, Gaussian 80% threshold, OCOG primary peak, narrow primary peak, threshold retrackers (TFMRA)

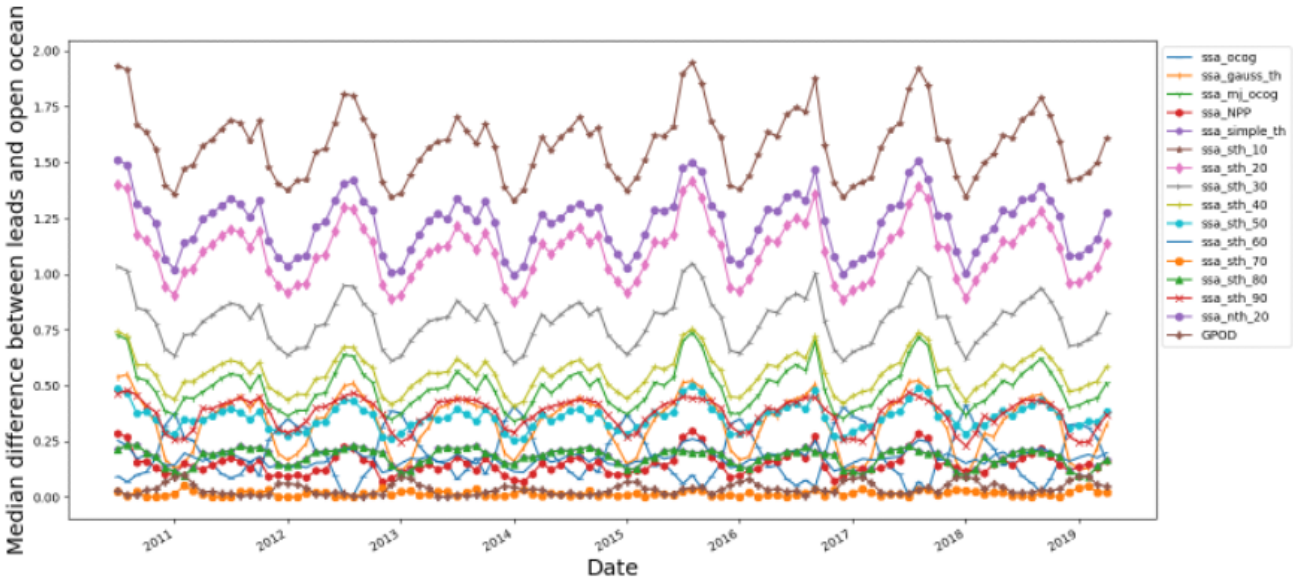

Figure 2. Median difference between open ocean and leads covering the South Polar Ocean for SAR mode only. The various empirical retrackers are (from legend): OCOG, Gaussian 80% threshold, OCOG primary peak narrow primary peak, threshold retrackers (TFMRA) from 10 to 90, and the physical SAMOSA+ retracker (GPOD).

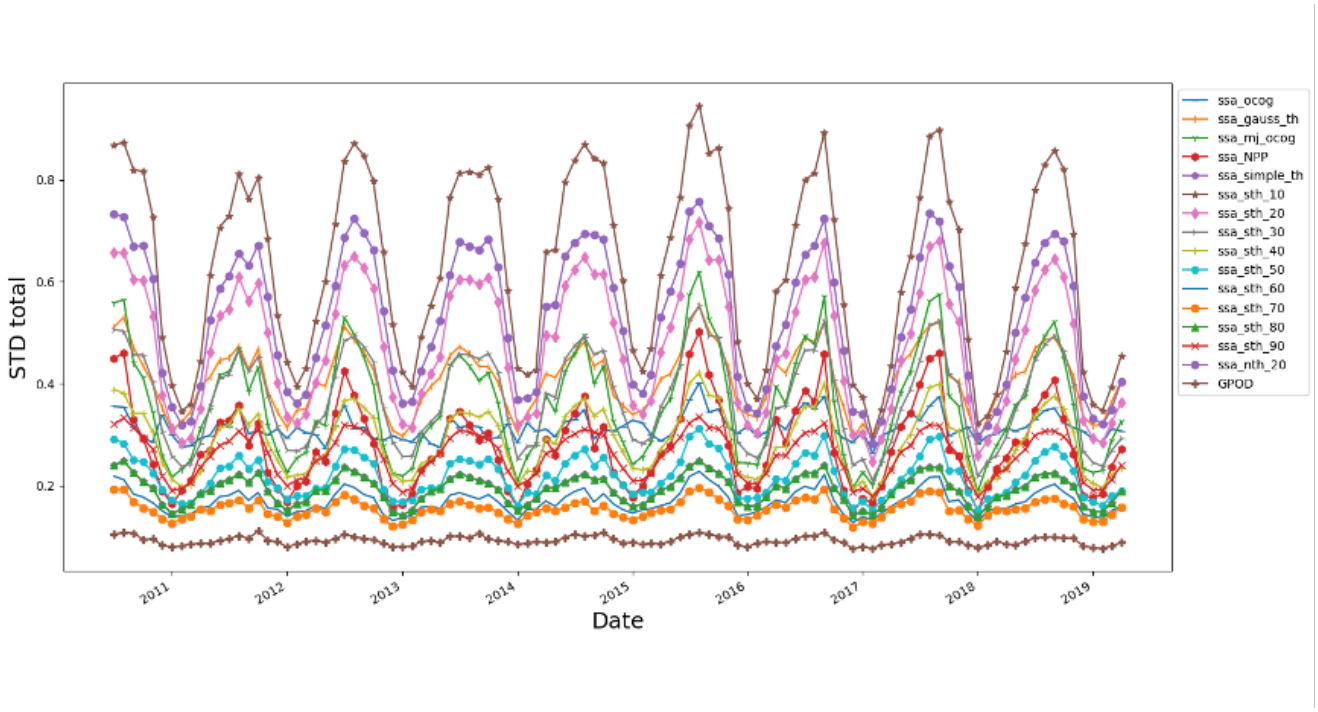

Figure 3. The total standard deviation of the monthly SLA. The various empirical retrackers are (from legend): OCOG, Gaussian 80% threshold, OCOG primary peak, narrow primary peak, threshold retrackers (TFMRA) from 10 to 90, and the physical SAMOSA+ retracker (GPOD).

References:

Dinardo, S., Restano, M., Ambrózio, A., and Benveniste, J.: SAR Altimetry processing on demand service for CryoSat-2 and Sentinel-3 at ESA G-POD, Proceedings of the 2016 conference on Big Data from Space, pp. 268–271, https://doi.org/10.2788/854791, 2016.

Dinardo, S., Fenoglio-Marc, L., Buchhaupt, C., Becker, M., Scharroo, R., Joana Fernandes, M., and Benveniste, J.: Coastal SAR and PLRM altimetry in German Bight and West Baltic Sea, Advances in Space Research, 62, 1371–1404, https://doi.org/10.1016/j.asr.2017.12.018, 2018.

2.1.2 Gridded Sea Level Product

```
netcdf cs_plus_antarctica_sea_level_DTU_v0.3 {
dimensions:
      date = 138 ;
      lon = 720;
      lat = 120;
```

```
variables:
     double sla(date, lon, lat) ;
     double err(date, lon, lat)  ;
     double sla_nodac(date, lon, lat)  ;
      double dot(date, lon, lat)  ;
      int64 date(date) ;
      double lon(lon) ;
      double lat(lat) ;
global attributes:
      :description ="CryoSat+ Antarctica Monthly
South Polar Ocean dataset" ;
      :history = "Created Thu Nov 24 11:01:01 2022" ;
      :version = "0.3 Thu Nov 24 11:01:01 2022" ;
      :source = "DTU Space" ;
      :contact = "S.K. Rose: stine@space.dtu.dk" ;

data:
…
}
```

2.1.3 Preparing the Gridded Sea Level Product

The main preparation of the data pre-gridding is performed and described in the *Product Validation Report_Along_Track* document. In this part of the study the following were done:
An offset between the three modes are calculated. This is done by comparing the median difference between observations within 50 km from each other in all modes.
Extreme values are removed (+/- 10m around median)
Median Absolute Deviation (MAD) outlier detection is applied
As a pre-cleaning, we are averaging cells of to overcome the sampling dissimilarity.

2.1.4 The Gridding

The gridding is done by Interpolation using ordinary kriging/collocation and is described in the *ATBD*. In the kriging routine an error estimate is obtained for each grid point which is related to the interpolation of data. In this case, data with a 10 cm of error is rejected and set to NaN.

2.1.5 Intercomparison

The processing of the monthly distribution of the SLA (Figure 4) revealed some issues with the SARIn mode of data (Figure 4(a)). They are stripy and could look like an issue with the tidal correction. It has not been possible to solve, instead a DTU post processing of the GPOD data is used to cover the SARIn data (Figure 4(b)). In the last panel, Figure 4(c), extreme values are removed and a MAD outlier detection is applied before gridding.
From the figure we see how the InterQuartile Range (IQR) improves in the processing steps from (a) to (c).

Figure 5 shows CS+ AO SLA monthly solutions and Figure 6 shows two examples of the DOT for January and July.

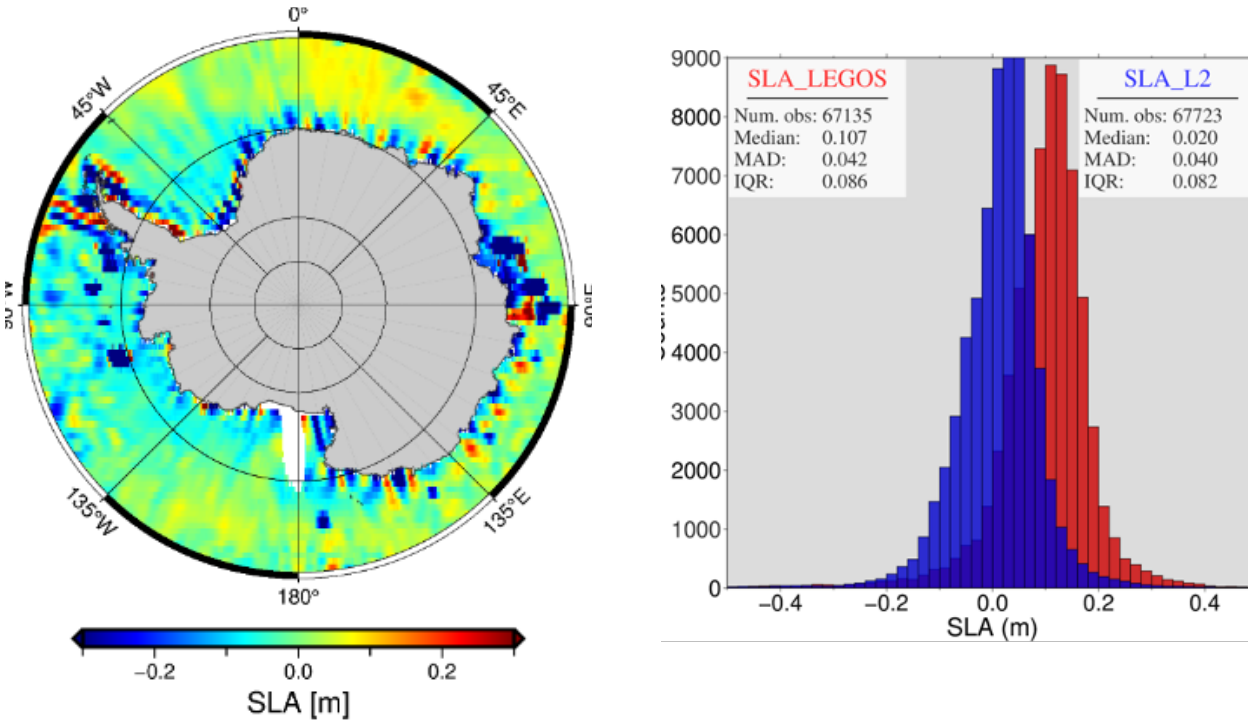

(a)

(b)

(c)

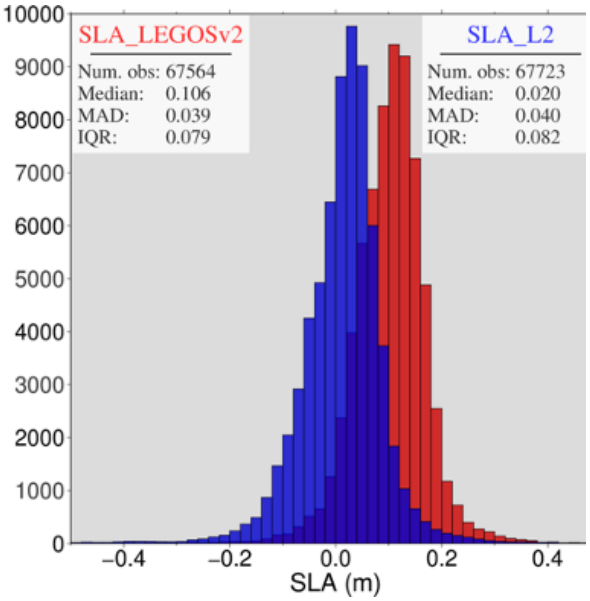

Figure 4. Processing steps improving the SLA. Data are shown from January, 2019, monthly

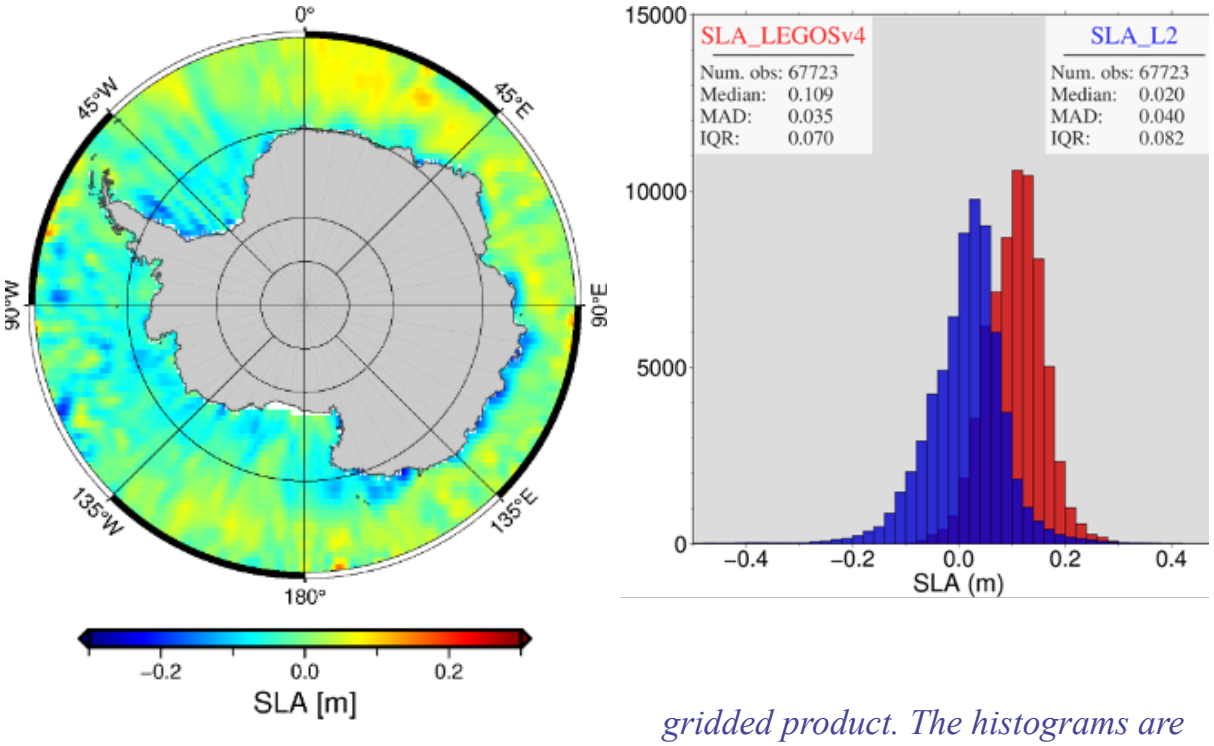

gridded product. The histograms are shown together with the CryoSat-L2 GDR product. In the maps the SLA is centred around zero.

Figure5. Monthly SLAs from January (top left) to December 2019 (bottom right).

Figure 6. Examples of monthly DOT for January 2019 (left), and July 2019 (right).

2.1.6

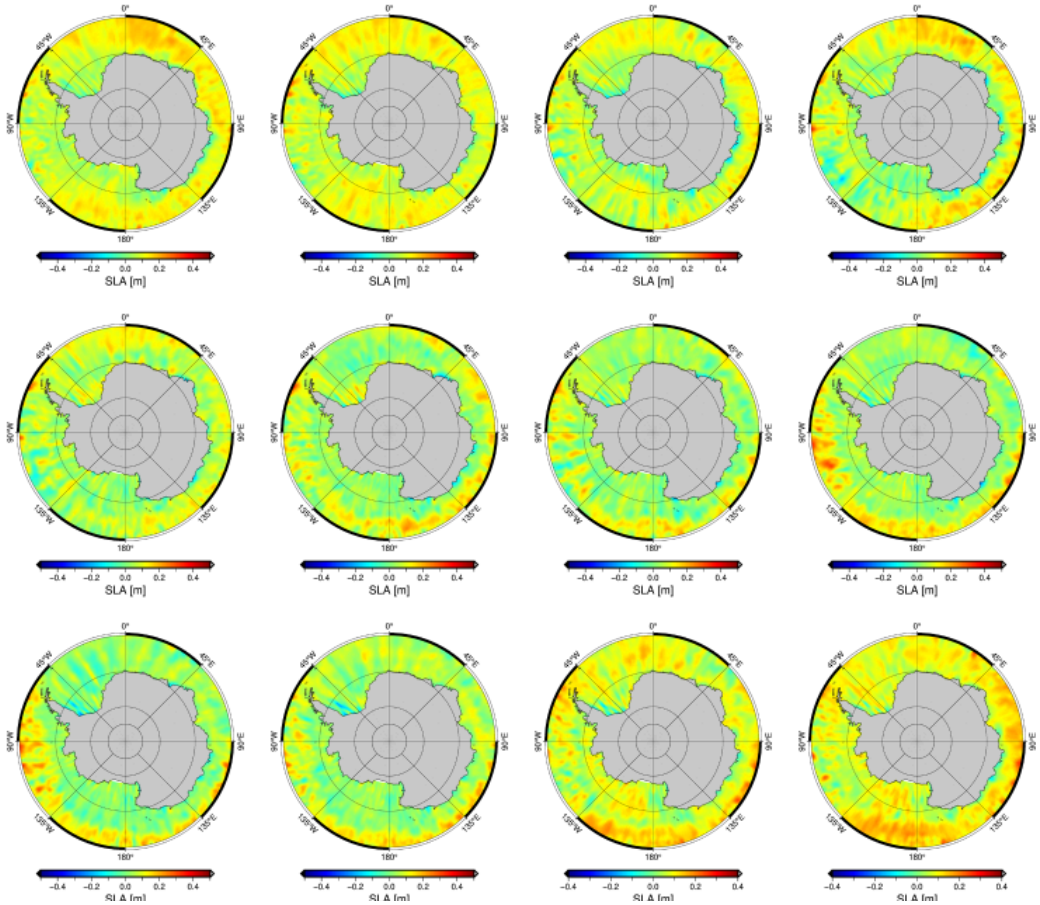

Validation

2.1.6.a Validation Against L2

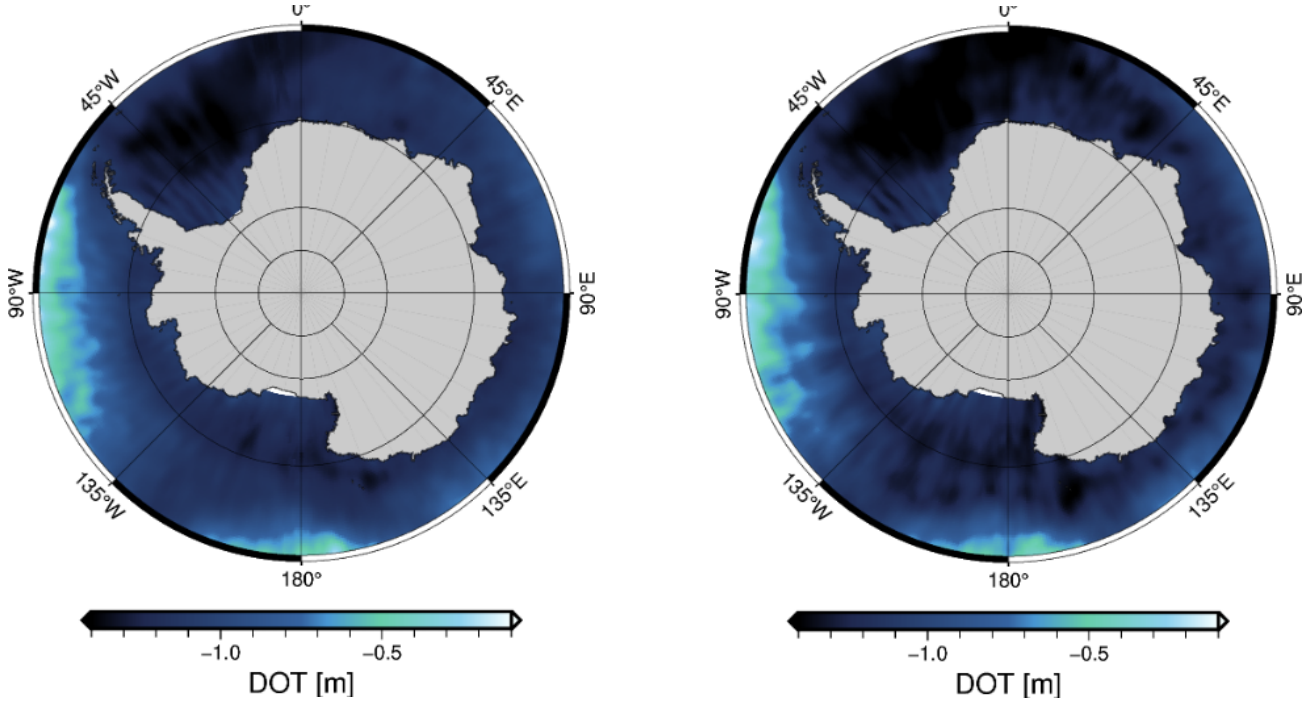

January and July are used as test months for comparing the SLA against the L2 GDR product (Figure 7). The corresponding histograms are shown in Figure 4(c). The main differences between the products are seen close to the coast. Figure 8 compares the mean of the whole year of data from the CS+ AO data and the L2 GDR product. Generally, the CS+ AO product is more smooth, probably due to the outlier detection.

L2 GDR CS+AO Difference

Jan

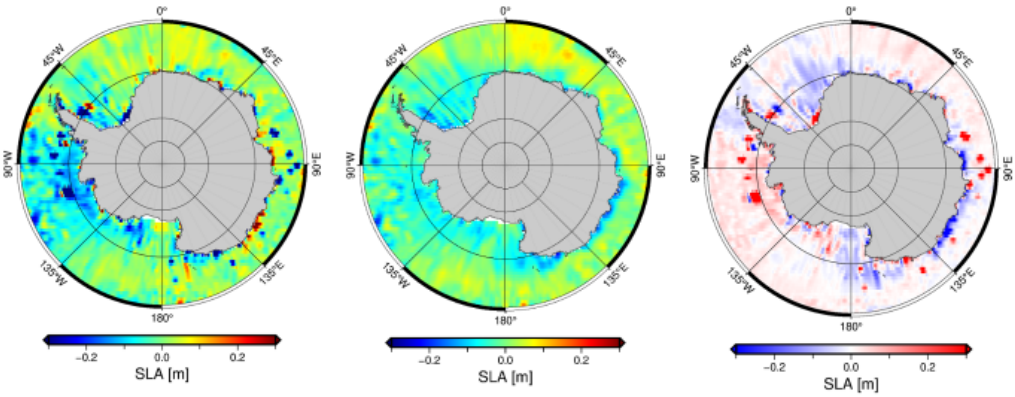

July

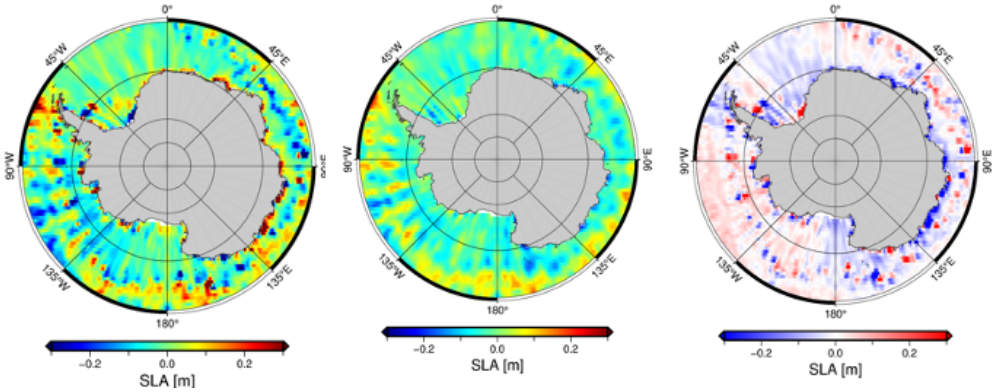

Figure 7.Comparing CS+ AO SLA data set against GDR L2 for January and July, 2019.

L2 GDR CS+AO

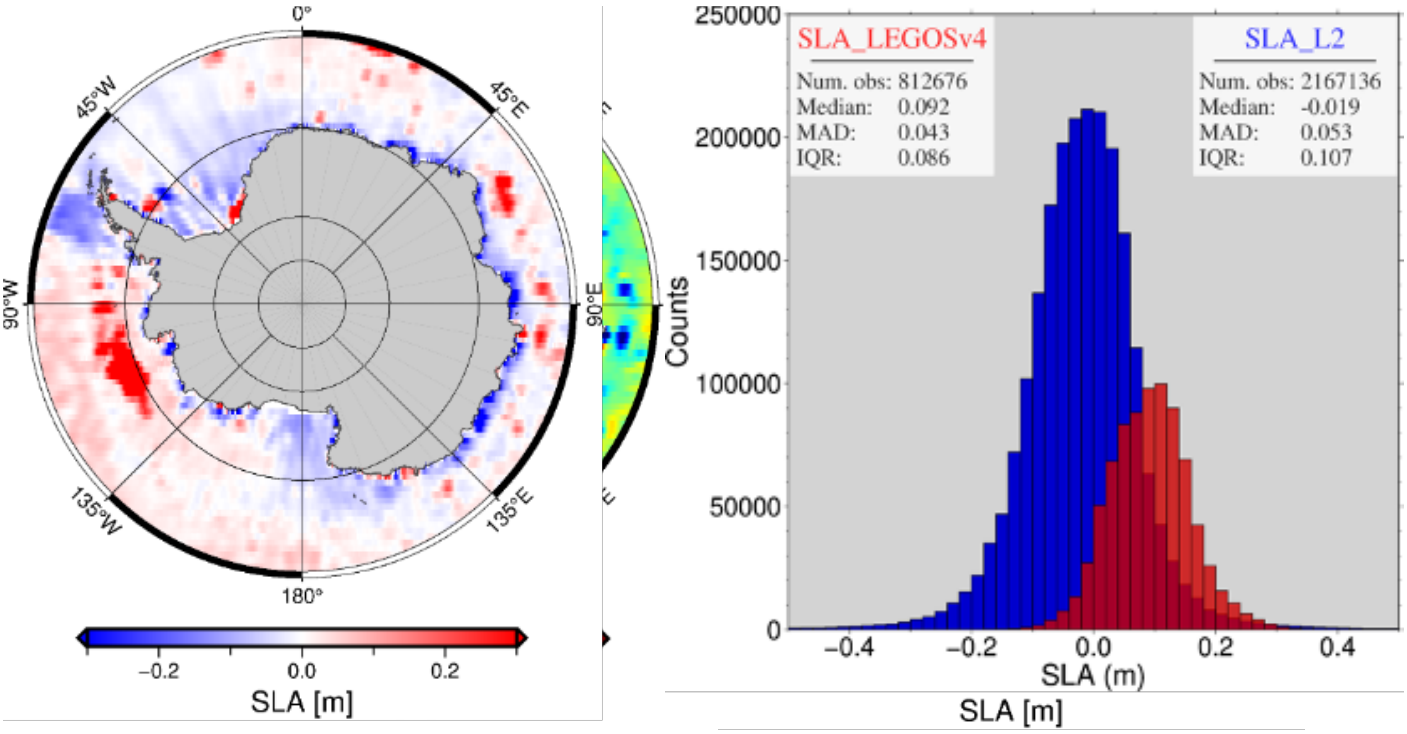

Figure 8. Yearly mean of all gridded SLAs for 2019 for L2 GDR, CS+ AO, the difference between the two products and the histogram distributions

2.1.6.b Validation against Tide Gauges

The tide gauges (Figure 9) are obtained from the Permanent Service for Mean Sea Level (PSMSL) [Holgate et al., 2013; PSMSL, 2018]. Comparing the altimetry to the tide gauges the atmospheric correction is not applied. Figure 10 shows the coverage in the CryoSat-2 L2 period. Only the Puerto Soberania tide gauge covers the CS AO test data set. In the comparison no correction to the Vertical land Movement (VLM) was applied. This effect can have both a seasonal effect and a trend, especially around large outlet glaciers. The positions are mainly in the zone of the SARIn mode. Generally, the tide gauges are in challenging locations for satellite altimetry comparison. We have chosen to make a monthly average in a 350 km radius around the tide gauge, as it favours the altimetry [Rose et. al., 2019].

Due to the fact that the test data set only covers 2019, the comparison to the tide gauges is difficult due to the limited overlap in time. Figure 11 shows the only comparison available. There is a weak correlation with a correlation coefficient of 0.45. The trends are shown on the figures, but the time period taking into account, it does not make sense to make the comparison.

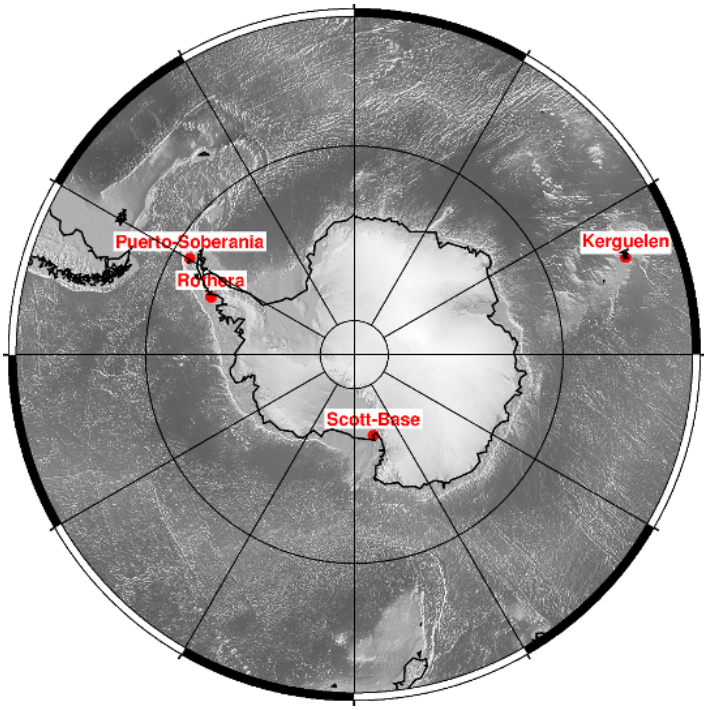

Figure 9. Location of tide gauges used in the comparison. The gauges are downloaded from PSMSL.

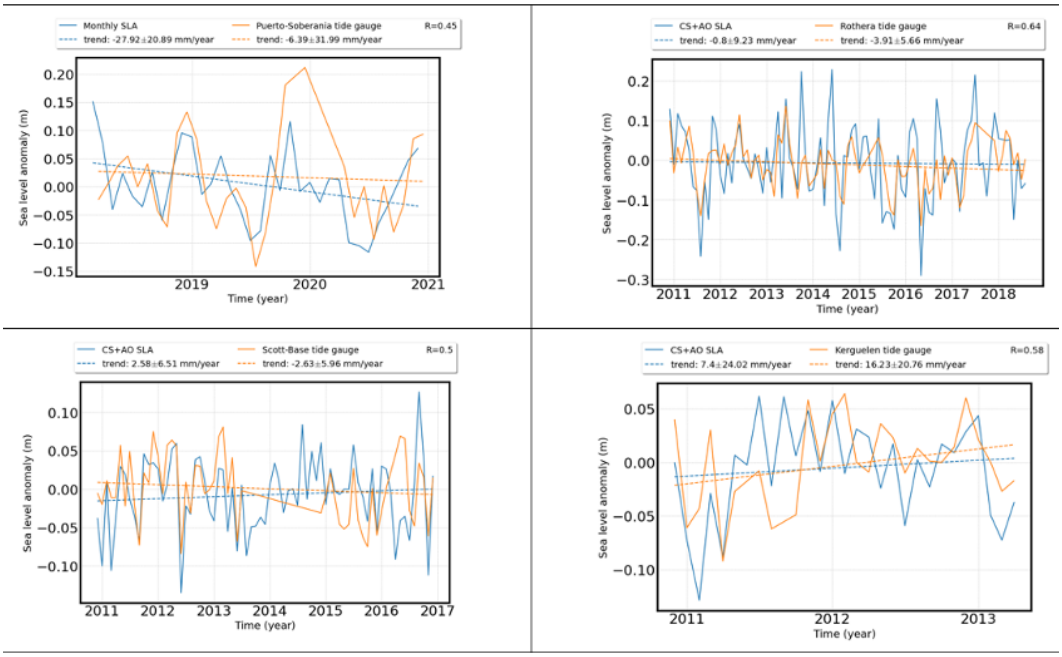

Figure 10. CryoSat-2 L2 comparisons to tide gauges.

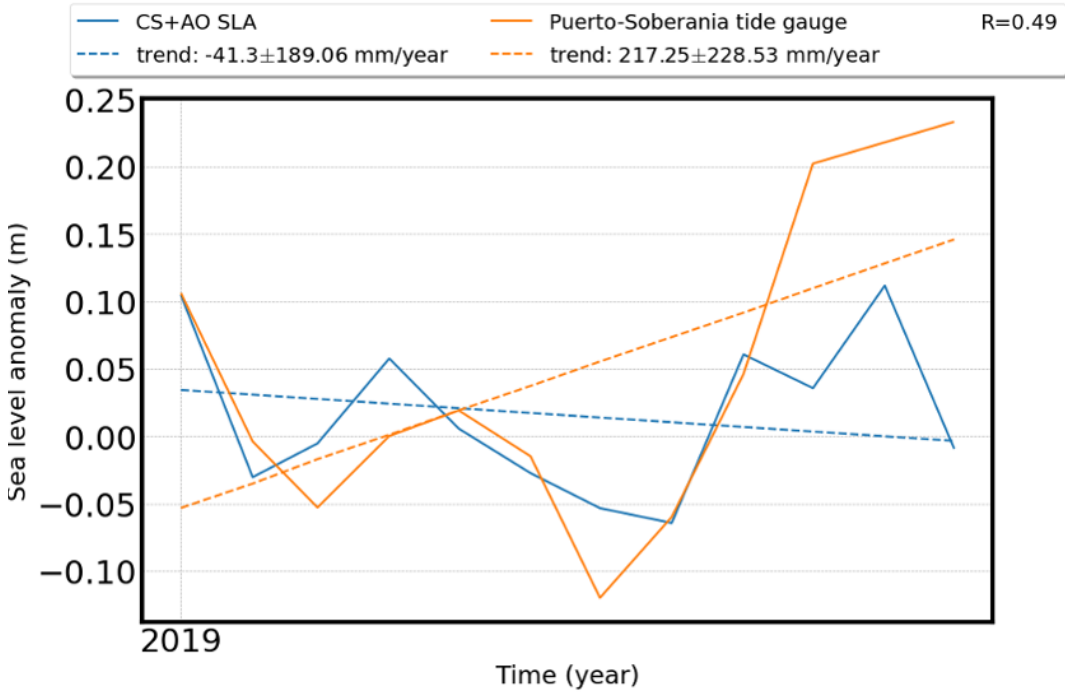

Figure 11. CS+ AO comparisons to the Puerto-Soberania tide gauge.

2.2. Sea Ice Freeboard and Sea Ice Thickness Product

The CSAO sea ice freeboard and thickness experimental product is a monthly gridded dataset for the 6 winter months (May to October) in 2019. To ensure a « user-friendly » interface only 5 variables are provided (with their uncertainties) : the sea level anomaly, the sea ice radar freeboard, the sea ice freeboard, the snow depth and the sea ice thickness. In the next section we describe the product and the methodology used to produce this dataset from along track calculations of surface heights.

2.2.1. Product organization, data format and parameter description

The sea ice freeboard and thickness CSAO experimental dataset is provided in 712 x 712 EASE2-grids with a 12.5 km pixel size. The format is NetCDF v.4.
The files are named as follows:

CS2_CSAO+_SIT_w25000_${year}${month}.nc,
(eg: *CS2_CSAO+_SIT_w25000_201906.nc).*

« w25000 » indicates that each pixel is a weighted mean of all the along-track measurement within a 25 km radius from the centre of the pixel.

The NetCDF files have the following dimensions :

```
    u = 712 ;
    v = 712 ;
    time = UNLIMITED ; // (1 currently)
    time_bounds = 2 ;
```

where u and v are the dimensions of the grid, time is the date of the mid-month and time_bounds are the first and the last date of the month. The 'time' dimension allows the merging all the monthly NetCDF files into one unique NetCDF file.

The global attributes are the following:

```
:title = "Sea ice Freeboard and Thickness experimental product
developed within the CryoSat+ Antarctic Ocean ESA project" ;
        :comment = "CryoSat-2 Altimetric freeboards are
computed at the LEGOS laboratory from ranges provided by the
SAMOSA+ physical retracker computed at the ESA GPOD
platform" ;
        :projection = "laea" ;
        :grid_type = "sp2ease" ;
        :lat_ts = 0 ;
        :lon_0 = 0 ;
        :pixel_size = 12500 ;
        :width = 8900000 ;
        :height = 8900000 ;
        :lat_0 = -90 ;
        :lat_min = -90 ;
        :lat_max = -49.9532037437005 ;
        :nb_pixels_x = 712 ;
        :nb_pixels_y = 712 ;
        :filtering = "distance weight" ;
        :range_filter = "25000" ;
        :contact = "sara.fleury@legos.obs-mip.fr,
florent.garnier@legos.obs-mip.fr" ;
        :institution = "ESA/LEGOS" ;
        :Conventions = "CF-1.6" ;
        :date_of_creation = "2022-10-04 09:43:13.500658" ;
        :production = "LEGOS" ;
        :copyright_statement = "Copyright ESA-CSAO+ project" ;
```

Table 1 below specifies the variables included in the files:

NetCDF variable name	Full name	Units	Short description
latitude	latitude	degrees_north	Latitude coordinates corresponding to the EASE2-Grid
longitude	longitude	degrees_east	Longitude coordinates corresponding to the EASE2-Grid
sla	Sea level anomaly	meters	Altimetric sea level anomy computed from the heights over the leads
sla_unc	Sea level anomaly uncertainty	meters	Uncertainty related to the sea level anomaly estimations.
freeboard_radar	Radar freeboard radar height	meters	Altimetric freeboard height measured from altimetry without correction due to the radar speed decreasing in snow
freeboard_radar_unc	Radar freeboard height uncertainty	meters	Uncertainty related to the radar freeboard estimations
freeboard_ice	Sea ice freeboard	meters	Altimetric freeboard height measured from altimetry taking into account the correction due to the radar speed decreasing in snow
freeboard_ice_unc	Uncertainties on sea ice freeboard	meters	Uncertainty related to the sea ice freeboard estimations
snow_depth	snow depth	meters	ASD Dual frequency Ka-Ku Snow depth dataset
snow_depth_unc	Uncertainty of snow depth	meters	Uncertainty related to the snow depth
sea_ice_thickness	sea ice thickness	meters	Sea ice thickness computed from the radar freeboard and the snow depth
sea_ice_thickness_unc	sea ice thickness uncertainty	meters	Uncertainty related to the sea ice thickness estimations

Table 1: Names and short description of the variables included in the sea ice freeboard and thickness CSAO experimental dataset

2.2.2. Description of the processing

The processing steps to compute and validate freeboard and sea ice thickness from altimetry are shown in Figure 12 below.

The next sections describe these different step, apart the retracker. Indeed, in the context of this project, we directly used the ranges computed by GPOD using the SAMOSA+ retracker. Also, since we apply the exact same methodology to compute the heights of leads and floes, the heights can be computed before the leads/floes classification.

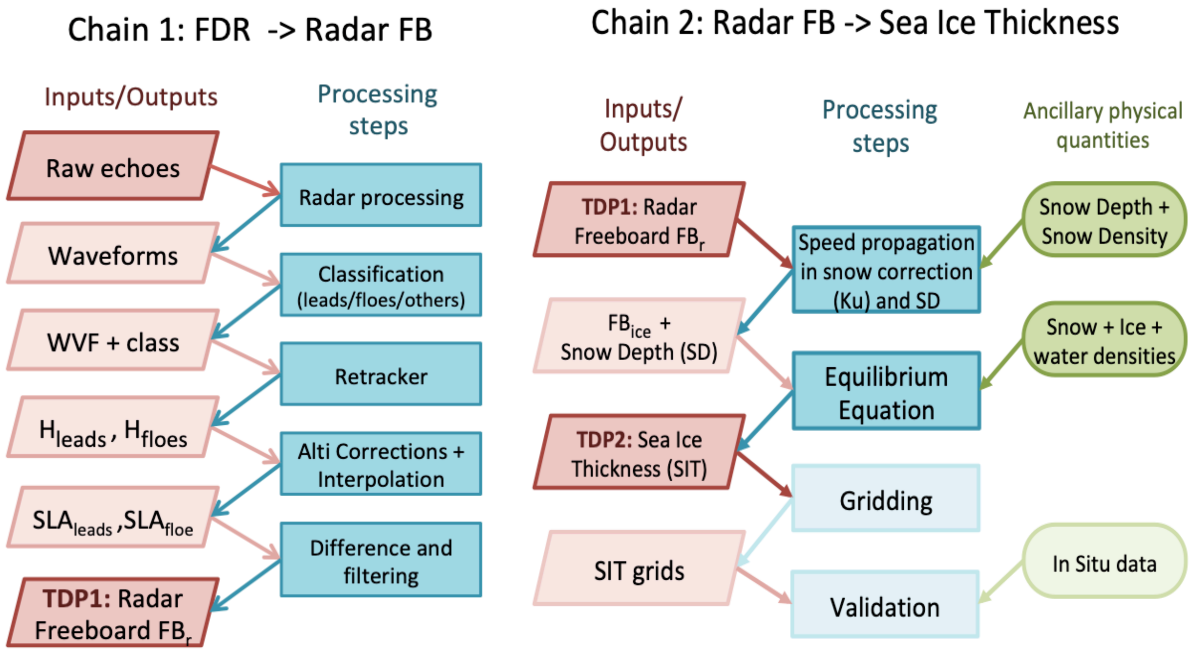

Figure 12 : Processing steps to compute radar Freeboard from altimetric waveforms (chain 1) and to compute the sea ice thickness from the radar freeboard up to validation (chain 2).

2.2.3. Along track processing of All Surface Anomalies (ASA)

At first, the surface level anomaly is computed along-track, without distinction of the surface type (floes, leads), providing the All Surface Anomaly (ASA).

The ASA (Eq.1) are derived from the ranges computed with The SAMOSA+ physical retracker at the ESA Grid Processing On Demand computing Sciences (GPOD) SARvatore chain (*Dinardo et al, 2016*), newly transferred to EarthConsole (https://earthconsole.eu). The Zero-Padding and Hamming window are the only processing options activated (consistently with the results of Laforge *et al 2019),* as it is the case for the PDGS version of CryoSat-2.

Surface anomaly = Alt – Range – MSS – Geophysical corrections (Eq. 1)

Alt is the altitude of the satellite (from the ESA CryoSat-2 Baseline D L2 product), the Range is calculated with SAMOSA+, the MSS is the mean sea surface given by the MSS_DTU_21 dataset. The following Geophysical corrections are used: the dry and wet tropospheric corrections, the ionospheric correction, the ocean tide , the solid earth tide, the geocentric pole tide, the Dynamical atmospheric correction (DAC) and, the inverted barometer correction and the sea state bias (ssb) such as :

Geophysical corrections = dry+ wet + iono + ocean tide + earth_tide + pole_tide + DAC + inv_bar + ssb

With :

dry_tropo_corr	ECMWF Atmospheric Dry Correction at 1 Hz (zero-altitude)
wet_tropo_corr	ECMWF Atmospheric Wet Correction at 1 Hz
iono_gim_corr	GIM Iono Correction at 1 Hz
dac_corr	Inverse Barometric Correction + Dynamic Atmospheric Correction
FES14b_equil_ocean_tide	FES2014b Ocean Equilibrium Tide
FES14b_long_period_ocean_tide	Ocean Long Period Tide
FES14b_load_ocean_tide	FES2014b Ocean Load Tide
solid_earth_tide_corr	Solid Earth Tide
polar_tide_corr	Pole Tide
sea_state_bias	Sea State Bias Solution at 1 Hz (Source: Jason2 CLS 2012)

It is important to note that all the corrections that are usually applied over open-ocean are used. In particular we have added the sea state bias. This is crucial to get continuity between open-ocean and ice-covered ocean. Indeed, without this correction, there is a discontinuity of several centimetres on the SLA at the sea ice margins. The different evaluations show that this option does not degrade the freeboard solution. Differences are very small and even tend to lightly reduce the standard deviation. On the other hand, the improvement in SLA is significant has shown Figure 13.

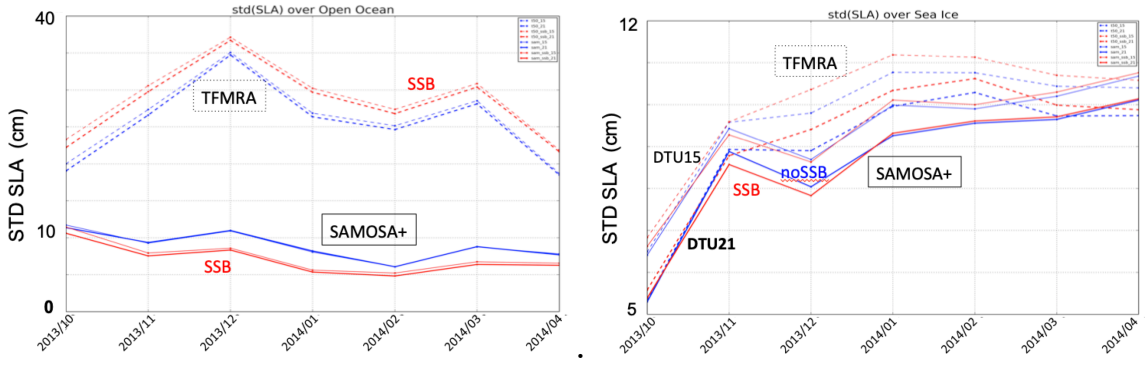

Figure 13: Impact of the retracking method (TFMRA in dotted lines, SAM+ in continuous lines), the Mea Sea Surface (DTU15 in thin lines, DTU21 in bold lines) and the sea state bias (no ssb is applied in blue, SSB applied in red) on the Standard Deviation of the SLA. Over open ocean on the left and over sea ice leads on the right. The best configuration is with the combination SAM+/DTU21/SSB. The SSB has a very negligible impact over sea ice.

Except for the ocean tide and the DAC and the SSB, all the geophysical corrections are provided by the ESA CryoSat-2 Baseline D L2 product. The ocean tide has been replaced by FES2014. The DAC is calculated from the MOG2D model and the SSB is coming from the model initially elaborated by CLS for Jason 2.

2.2.4. Leads/floes classification

The classification of lead/floes is based on the Pulse Peakiness (PP) criteria. The surface is considered as a lead for $PP > 0.3$ and as a floe when $PP < 0.1$. Values between 0.1 and 0.3 are discarded. In a second step, we also filtered out the Off-Nadir and Side-Lobes data using a fast 2D retracker and, if available, the Range Integrated Power (RIP).

2.2.5. Along track processing of All Surface Anomalies (ASA)

Sea level anomalies (SLA)

In order to estimate the SLA under sea ice, the ASA measured over the leads are interpolated under the floes. In a first step, the SLA measured over the leads are filtered using an along-track running 3 STD filter to remove outliers (ie, data that are not included in the range of the mean SLA ± 3 × the SLA standard deviation are discarded). The remaining SLA are then smoothed with a rolling mean in a 12.5 km window. A linear interpolation is then applied to estimate sea level anomalies under the floes. Finally, a last rolling mean smoothing, with a 12.5 km window, is applied in order to lead to the variable *SLA_smooth*.

Ice level anomalies (ILA)

The anomaly of sea ice heights (or ice level anomalies) is based on the same methodology but using the ASA over the floes. This symmetrical approach allows to obtain interpolated estimations of the height of the floes (ILA) over the leads, as it is the case for the SLA. We finally obtain the variable *ILA_smooth*.

2.2.6. Along track processing of radar and sea ice freeboard.

The along track radar freeboard is simply the difference between the heights of the sea ice and the sea level anomalies (Eq.2), obtained from the methodology presented in the previous section.

$$\mathrm{FBr} = \mathrm{ILA\_smooth} - \mathrm{SLA\_smooth} \quad \text{(Eq. 2)}$$

Based on the National Snow and Ice Data Center (NSIDC-0051) dataset of the sea ice index archive, freely available at ftp://sidads.colorado.edu/DATASETS/NOAA/G02135, data are removed when the sea ice concentration is less than 50%.

The computation of the sea ice freeboard take into account the decreasing of the radar speed velocity when it penetrates into the snow pack following *Ulaby et al, 1986* :

$$Cs = c \times \left(1 + 0{,}51 \times \rho_s\right)^{(-1{,}5)} \quad \text{(Eq. 3)}$$

With Cs is the velocity in snow and c is the velocity in vacuum.

It leads to an expression of the sea ice freeboard Fb such as (*Kwok and Cunningham, 2015)* :

$$\mathrm{FB} = \mathrm{FBr} + SD\left(1 - \left(1 + 0{,}5\rho_s\right)^{-1{,}5}\right) \text{ (Eq. 4)}$$

With SD the snow depth (see next section) and ρ_s is the density of snow.

2.2.7. Snow depth

The snow depth product provided in the CSAO experimental dataset is a replica of the ASD dual-frequency Ka-Ku snow depth product developed at the LEGOS laboratory. It is fully described in *Garnier et al, 2021*. The methodology relies on the difference of penetration into the snow pack of the Ka-band frequency of the SARAL/AltiKa and the Ku-band frequency of the CryoSat-2/SIRAL altimeter. The assumption is that the Ka-band radar echo reflects on the top of the snow pack and that the Ku-band radar reflects at the interface between the ice and the snow. AltiKa operating in Low Resolution Mode, it is necessary to use the pLRM processing of CryoSat-2 waveforms. The pLRM version of the waveforms are provided within the the GOP ESA Baseline C product. The SARAL data are coming from the CNES SGDR v2.1 product.

For each satellite we calculate along track radar freeboards using the methodology previously described. Apart from the use of (p)LRM waveforms, the only difference is that the ranges are calculated using a TFMRA retracker, with a 50% threshold. We then calculate a « radar » snow depth (SD*r*) from the difference between the freeboards of SARAL and CryoSat-2:

$$SDr = \mathrm{FB}_{ka} - \mathrm{FBr}_{ku} \quad \text{(Eq. 5)}$$

Note that the hypothesis of non-penetration of the ka-band within the snow, the radar freeboard is equal to the sea ice freeboard for SARAL.
Taking into account the decreasing of radar velocity in the snow pack, the snow depth SD is given by Eq.6 :

$$SD = \mathrm{SDr} \times \left(1 + 0{,}51 \times \rho_s\right)^{(-1{,}5)} \quad \text{(Eq. 6)}$$

Note that the use of two satellites prevents us from calculating along track snow depths. The difference between SARAL and CryoSat-2 freeboards therefore requires to grid the data (cf. section 6). The snow depth is then a monthly gridded product.

2.2.8. Sea Ice Freeboard to Thickness conversion

The radar freeboard is converted into sea ice thickness using the hydrostatic equilibrium between the snow covered sea ice and the ocean (*Laxon et al., 2003)*:

$$SIT = \frac{\rho_w \mathrm{FB} + \rho_s SD}{\rho_w - \rho_i} \quad \text{(Eq. 7)}$$

In this equation, ρ_w, ρ_s and ρ_i represent respectively the sea water, the snow and the ice densities. FB is the sea ice freeboard (corrected from the slow wave propagation in the snow pack), and *SD* is the snow depth.

Sea water, sea ice and snow densities

As for the Arctic, the sea water density ρ_w is set to a constant value of 1024 kg.m^{-3} (*Wadhams et al., 1992*). In the Antarctic, we consider that the sea ice is only composed of First Year Ice. The snow ρ_s and sea ice densities ρ_i only depend on the month as proposed in *Kurtz et al, 2012:* in May, the sea ice density is set to 900 kg.m^{-3} and the snow density is 320 kg.m^{-3}. In October, the sea ice density is set to 875 kg.m^{-3} and the snow density is 340 kg.m^{-3}. For all other months of winter, the sea ice density is set to 900 kg.m^{-3} and the snow density is 350 kg.m^{-3}.

Gridding

Due to the specificities of the ASD snow depth dataset, the Sea ice thickness is derived from monthly gridded radar freeboard estimations.
The current gridding technique used to construct monthly radar freeboard maps consists of a weighted averaging of the along-track measurements points within a radius R=25 km from the centre of each pixel. The weight is the inverse of a Gaussian distribution of the distance from the centre of the pixel. The final dataset is on EASE2 grids with a pixel resolution of 12.5 km, on a monthly basis for the six month of winter (from May to October).

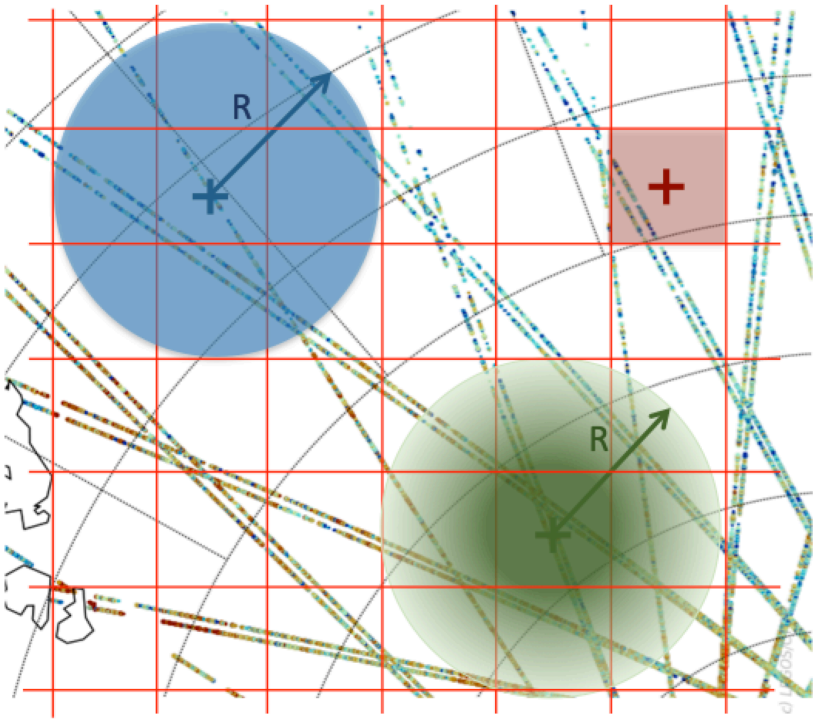

Figure 14: Different gridding technics: In red the simple binning which is the mean (or the median) of the all measurements within the pixel. In blue all the measurements within a given radius from the centre of the pixel are taken into account (radius of influence). It allows to better smooth from one pixel to another. In green the mean is weighted by the distance to the centre of the pixel. It is this last solution that is used to grid the product.

2.2.9. Uncertainties

To estimate uncertainties, we assume that errors are unbiased, uncorrelated and follow a Gaussian law. We can then apply the following Gaussian propagation law:

$$\varepsilon^2_{f(x_i)} = \sum_{i=1}^{n} \left(\frac{\partial \left(f(x_i) \right)}{\partial x_i} \right)^2 \varepsilon^2_{x_i} \qquad (8)$$

Uncertainties on surface anomalies

As operated over ocean surfaces, the uncertainty associated to individual surface height measurements can be estimated from the local (i.e. within along-track sections of 25 km) standard deviation of surface height estimated in leads. Regarding ice floes, the surface height standard deviation is strongly impacted by the freeboard variability and can not be used to estimate uncertainties. Then, we make the assumption that the individual uncertainty of surface height over ice floes is identical to the individual uncertainty over leads.

The first step consists in estimating the average value of the Sea Level Anomaly standard deviation (σ_{SLA}) in each along-track section of 25 km. To take into account the impact of the data averaging that reduces the uncertainty within the 25 km averaged sections, the uncertainties associated to the surface height of leads and floes is considered as Gaussian and is estimated as follows:

$$\varepsilon_{H_{floe}}^2 = \frac{{\sigma_{SLA}}^2}{N_{floe}} \text{ and } \varepsilon_{H_{lead}}^2 = \frac{{\sigma_{SLA}}^2}{N_{lead}} \quad (9)$$

Where $N_{floe}$and N_{lead} *are* the number of floes and leads within each section of 25 km.

Uncertainties on radar freeboard

Using equation (8) and (9) the radar freeboard uncertainty provided in the products is then :

$$\epsilon_{fb_{radar}} = \sqrt{\varepsilon_{H_{floe}}^2 + \varepsilon_{H_{lead}}^2} \quad (10)$$

Uncertainties on sea ice freeboard

The freeboard ice Fb corresponds to the radar freeboard corrected from the slow wave propagation in the snow pack.

Combining equation (4) with the Gaussian approximation (8) the freeboard ice uncertainty $\epsilon_{fb_{ice}}$ is then:

$$\epsilon_{fb_{ice}} = \sqrt{\epsilon_{fb_{radar}}^2 + \left(\epsilon_{sd} \times A\right)^2 + \left(\epsilon_{\rho_s} \times sd \times B\right)^2} \quad (11)$$

with $A = 1 - \left(1 + 0{,}51 \times \rho_s\right)^{(-1{,}5)}$ and $B = -1{,}5 \times 0{,}51 \times \left(1 + 0{,}51 \times \rho_s\right)^{(-2{,}5)}$

ϵ_{ρ_s} is the uncertainty of the ice density uncertainty. It is set to 3.2 $kg.m^{-3}$ (see tab>>>>>>>

$\epsilon_{fb_{radar}}$ is calculated following equation (10) and ϵ_{sd} is the snow depth uncertainty (see below).

Uncertainties on snow depth.

We calculate the freeboard uncertainties for SARAL and CryoSat-2 using equations 10 and 11. With the Gaussian approximation (8) approximation (), we then have :

$$\epsilon_{sd} = \sqrt{\left(\epsilon_{sdr} \times C\right)^2 + \left(sdr \times B \times \epsilon_{\rho_s}\right)^2} \quad (15)$$

with $C = \left(1 + 0{,}51 \times \rho_s\right)^{(-1{,}5)}$. B is defined above. The snow depth uncertainty is $\epsilon_{sdr} = \sqrt{\left(\epsilon^2_{fb_{ka}} + \epsilon^2_{fb_{ku}}\right)}$ where $\epsilon^2_{fb_{ka}}$ and $\epsilon^2_{fb_{ku}}$ are calculated following equation 9 and 10.

Uncertainties on sea ice thickness.

To derive Sea Ice Thickness uncertainties, it is necessary to take into account the uncertainties related to the freeboard measurement as well as the uncertainties related to the freeboard-to- derived from equation (x) with the approximation (x):

$$\epsilon^2_{SIT} = \left(\rho_w D^{-1}\%\right)^2 \epsilon^2_{sd} + \left(\rho_w D^{-1}\right)^2 \epsilon^2_{fb_{ice}} + \left(fb_{ice}\rho_w D_2^{-1} + \rho_{sd} D_2^{-1} sd\right)^2 \epsilon^2_{\rho_i} + \left(\left(sd D^{-1}\right)^2 \epsilon^2_{\rho_{sd}}\right) \quad (16)$$

Note that ε_{ρ_w} is very small and therefore neglected.

The uncertainties of snow density, ice density and sea water density (respectively $\varepsilon_{sd}, \varepsilon_{\rho_i}$, and ε_{ρ_s} are provided in Table 2. Note that in the absence of values specific to the Antarctic we keep the values commonly used in the Arctic. These uncertainties are very likely to be underestimated.

Parameters	Typical value	Uncertainty	Reference
Snow density	*320*-350 $kg.m^{-3}$	3.2 $kg.m^{-3}$	[Warren et al., 1999]
Ice density	*875*-900 $kg.m^{-3}$	35.7 $kg.m^{-3}$	[Alexandrov et al., 2010]
Sea water density	1024 $kg.m^{-3}$	0.5 $kg.m^{-3}$	[Wadhams et al., 1992]

Table 2: Table summarizing the typical values of snow depth, snow density, ice density and sea water density as well as the associated uncertainties.

3. Dataset Access

The Experimental Datasets can be freely downloaded from the CSAO website

http://cryosat.mssl.ucl.ac.uk/csao/

4. References

Alexandrov, V., Sandven, S., Wahlin, J., & Johannessen, O. M. (2010). The relation between sea ice thickness and freeboard in the Arctic. The Cryosphere, 4(3), 373-380.

Andersen, O. B., Abulaitijiang, A., Zhang, S., and Rose, S. K.: A new high resolution Mean Sea Surface (DTU21MSS) for improved sea level monitoring, EGU General Assembly 2021, online, 19–30 Apr 2021, EGU21-16084, https://doi.org/10.5194/egusphere-egu21-16084, 2021.

Auger, M., Prandi, P. and Sallée, J.B., 2022. Southern ocean sea level anomaly in the sea ice-covered sector from multimission satellite observations. Scientific Data, 9(1), pp.1-10.

Dinardo, S.; Restano, M.; Ambrózio, A.; Benveniste, J. SAR altimetry processing on demand service for CryoSat-2 and Sentinel-3 906 at ESA G-POD. In Proceedings of the Proceedings of the 2016 conference on Big Data from Space (BiDS'16), Santa Cruz de 907 Tenerife, Spain, 2016, pp. 15–17.

Garnier, F., Fleury, S., Garric, G., Bouffard, J., Tsamados, et al (2021). Advances in altimetric snow depth estimates using bi-frequency SARAL/CryoSat-2 Ka/Ku measurements (2021). The Cryosphere, 1-40.

Guerreiro, K., Fleury, S., Zakharova, E., Rémy, F., and Kouraev, A.: Potential for estimation of snow depth on Arctic sea ice from CryoSat-2 and SARAL/AltiKa missions, Remote Sensing of Environment, 186, 339–349, 2016.

Knudsen, P., Andersen, O., & Maximenko, N. (2019). A new ocean mean dynamic topography model, derived from a combination of gravity, altimetry and drifter velocity data. Advances in Space Research, 1–13. https://doi.org/10.1016/j.asr.2019.12.001

Kurtz, Nathan T., and Thorsten Markus. "Satellite observations of Antarctic sea ice thickness and volume." Journal of Geophysical Research: Oceans 117.C8 (2012).

Kwok, R., & Cunningham, G. F. (2015). Variability of Arctic sea ice thickness and volume from CryoSat-2. Philosophical Transactions of the Royal Society A: Mathematical, Physical and Engineering Sciences, 373(2045), 20140157.

Laforge, A., Fleury, S., Dinardo, S., Garnier, F., Remy, F., Benveniste, J., ... & Verley, J. (2021). Toward improved sea ice freeboard observation with SAR altimetry using the physical retracker SAMOSA+. Advances in Space Research, 68(2), 732-745.

Laxon, S., Peacock, N., and Smith, D.: High interannual variability of sea ice thickness in the Arctic region, Nature, 425, 947–950, 2003

Permanent Service for Mean Sea Level (PSMSL), 2022, "Tide Gauge Data", Retrieved 25 April 2022 from http://www.psmsl.org/data/obtaining/.

Simon J. Holgate, Andrew Matthews, Philip L. Woodworth, Lesley J. Rickards, Mark E. Tamisiea, Elizabeth Bradshaw, Peter R. Foden, Kathleen M. Gordon, Svetlana Jevrejeva, and Jeff Pugh (2013) New Data Systems and Products at the Permanent Service for Mean Sea Level. Journal of Coastal Research: Volume 29, Issue 3: pp. 493 – 504. doi:10.2112/JCOASTRES-D-12-00175.1.

Rose, S. K., Andersen, O. B., Passaro, M., Ludwigsen, C. A., & Schwatke, C. (2019). Arctic ocean sea level record from the complete radar altimetry era: 1991-2018. Remote Sensing, 11(14). https://doi.org/10.3390/rs11141672

Ulaby, F., Moore, R. K., and Fung, A. K.: Microwave remote sensing: Active and passive. Volume 3 – From theory to applications, Addison-Wesley, Theory to Applications, 997 pp., 1986

Wadhams, P.; Tucker III, W.; Krabill, W.B.; Swift, R.N.; Comiso, J.C.; Davis, N. Relationship between sea ice freeboard and draft in 989 the Arctic Basin, and implications for ice thickness monitoring. Journal of Geophysical Research: Oceans 1992, 97, 20325–20334.